Journal of Structural Geology 33 (2011) 1010–1022

Contents lists available at ScienceDirect

Journal of Structural Geology

journal homepage: www.elsevier.com/locate/jsg

Magnetic anisotropy reveals Neogene tectonic overprint in highly strained carbonate mylonites from the Morcles nappe, Switzerland

Bjarne S.G. Almqvist [a,*], Ann M. Hirt [a], Marco Herwegh [b], Bernd Leiss [c]

[a] Institute of Geophysics, ETH Zurich, Sonneggstrasse 5, CH-8092 Zurich, Switzerland
[b] Institute of Geological Sciences, Universität Bern, Baltzerstrasse 1+3, CH-3012 Bern, Switzerland
[c] Geoscience Centre, University of Göttingen, Goldschmidtstrasse 3, 37077 Göttingen, Germany

ARTICLE INFO

Article history:
Received 15 October 2010
Received in revised form
25 January 2011
Accepted 13 February 2011
Available online 19 February 2011

Keywords:
Anisotropy of magnetic susceptibility
Diamagnetic anisotropy
Paramagnetic anisotropy
Magnetic sub-fabric
Morcles nappe
Tectonic overprint

ABSTRACT

The anisotropy of magnetic susceptibility (AMS) has been measured with low- and high-field methods, in deformed carbonate rocks along the Morcles nappe shear zone (Helvetic Alps). High-field measurements at room temperature and 77 K enable the separation of the ferrimagnetic, paramagnetic and diamagnetic anisotropy. The ferrimagnetic sub-fabric is generally insignificant in these rocks, contributing less than 10% to the total AMS. AMS results for both the separated diamagnetic and paramagnetic subfabrics are consistent with the regional shear movement in the late-stage formation of the Helvetic nappes, as seen in the Morcles nappe, whose inverted limb indicate shear displacement towards the northwest. The diamagnetic anisotropy correlates well quantitatively with the calculated magnetic anisotropy based on the calcite texture. There is a gradational change in the degree of anisotropy related to the strain gradient along the shear zone. A more complex magnetic fabric, resulting from partial overprinting due to displacement along the Simplon–Rhône fault, is evident at one site near the root zone of the nappe. Partial overprinting of the magnetic fabric appears to have taken place in two locations farther up the shear zone as well. This late phase deformation is associated with recent exhumation of the Mont Blanc and Belledonne external massifs and orogen parallel extension, and is reflected by the AMS. Rocks with bulk susceptibility ~0 SI, and simple mineral compositions are ideal for low temperature high-field torque, as this method helps to enhance the paramagnetic susceptibility and anisotropy, which may otherwise be masked by the mixed magnetic contributions of the composite magnetic fabric.

1. Introduction

The magnetic susceptibility of a rock sample is the sum of all constituent minerals, and the magnetic anisotropy arises from the grain shape (i.e., ferrimagnetic minerals) and crystal-preferred orientation of the minerals. But the contribution to the total susceptibility and anisotropy is dependent on the magnetic properties of the individual phases. This can lead to a complex relationship between the anisotropy of magnetic susceptibility (AMS) and the mineral fabric. As a result the AMS may be due to the superposition of more than one magnetic fabric (e.g., Kligfield et al., 1977; Hrouda, 1979; Goldstein, 1980; Borradaile, 1988; Hamilton et al., 2004; Borradaile and Jackson, 2010). Almqvist et al. (2010) addressed this problem for carbonate rocks from the Morcles Nappe, where they showed that the degree of anisotropy reflects the combination of a paramagnetic anisotropy countering a diamagnetic anisotropy. Superposition of magnetic fabrics can also result from a mixture of primary fabrics, such as bedding, and the secondary fabrics produced by one or several tectonic events (e.g., Kligfield et al., 1981, 1983; Daly and Henry, 1983; Henry and Daly, 1983; Hirt et al., 1988; Park et al., 1988; Borradaile and Hamilton, 2004).

In general AMS studies concentrate on paramagnetic and ferromagnetic (*s.l.*) minerals, since their susceptibilities are high; typically 10^{-5}–10^{-3} SI for paramagnetic minerals and $>5 \times 10^{-3}$ SI for ferromagnetic minerals. Diamagnetic minerals such as calcite and quartz (-12 to -14×10^{-6} SI), which have comparatively much weaker susceptibility, have received less attention. Only a few exceptions exist where workers have addressed the diamagnetic anisotropy of rocks comprising nearly pure calcite or quartz (Owens and Rutter, 1978; Borradaile et al., 1999; deWall et al., 2000; Hirt et al., 2000). However, quartz and calcite commonly occur as matrix minerals in deformed rocks and their crystallographic preferred orientation (CPO) reveal useful information about the conditions and mechanisms that are active during deformation.

* Corresponding author. Geological Institute, ETH-Zurich, Sonneggstrasse 5, CH-8093 Zurich, Switzerland.
E-mail address: bjarne.almqvist@erdw.ethz.ch (B.S.G. Almqvist).

0191-8141/$ – see front matter © 2011 Elsevier Ltd. All rights reserved.
doi:10.1016/j.jsg.2011.02.002

Because the magnetic fabric directly reflects the texture of a rock containing paramagnetic and diamagnetic minerals, valuable information can be extracted from calcite and quartz if their magnetic anisotropy can be isolated. Recent advances in instrumentation and the possibility of measurements at 77 K, in addition to room temperature permit the separation of magnetic anisotropy in rocks that contain mixtures of ferrimagnetic (*s.s.*), paramagnetic and diamagnetic minerals (Martín-Hernández and Hirt, 2001; Schmidt et al., 2007a). Schmidt et al. (2009) used these techniques to separate the diamagnetic and paramagnetic anisotropy in synthetic aggregates composed of calcite and muscovite, and Almqvist et al. (2009) applied the method in an initial study of the Morcles nappe on a regional scale. In the present work diamagnetic and paramagnetic fabrics in deformed carbonate rocks are separated in order to better understand the deformation gradient and tectonic history along the major shear zone that is located in the overturned limb of the Morcles nappe.

1.1. Geological setting and samples

The Morcles nappe is located in southwest Switzerland, and is the basal fault in the Helvetic Nappe stack (Fig. 1). The kinematic evolution of the nappe stack took place by successive emplacement of nappes from top to bottom with the Morcles nappe forming last (Collet, 1927; Trümpy, 1980; Ramsay, 1981; Ramsay et al., 1983; Dietrich and Durney, 1986). The nappe stack plunges towards the northeast, where the base of the nappes goes from elevations as high as 2000 m down to the so-called Rawyl-depression (Ramsay, 1981). The thrust contact of the Morcles nappe overlies basement rocks of the Aiguilles Rouges massif, and the contact between basement rocks and the overlying Morcles nappe is defined by a shear zone, along which the nappe has been thrust 10–12 km towards the northwest (Goy-Eggenberger, 1998). Due to the high shear strain ($\gamma > 100$) in the shear zone, the bedding (S_0) and tectonic foliation (S_1) are sub-parallel (Ramsay et al., 1983). The most proximal portion of the shear zone in the southeast has been displaced by the Rhône–Simplon fault towards the west-southwest (Seward and Mancktelow, 1994), and is located presently north of the town Martigny. One sample locality from this location is referred to as Martigny and is shown in Fig. 1a.

The Morcles nappe has a well-developed mylonitic foliation with the stretching lineation parallel to the long-axis of the finite strain ellipsoid (Durney, 1972). The orientation of lineation in rocks, however, is observed to gradually rotate anti-clockwise with time. The oldest stretching lineation is oriented north–south, and is found in the normal limb of the nappe. A subsequent NW–SE stretching lineation is associated with the inverted limb, showing the transport direction of the nappe stack. A late-stage NE–SW stretching lineation is observed in locations of the nappe root zone (Dietrich and Durney, 1986); the latter stage NE–SW stretching lineation overprints the earlier NW–SE and N–S trending lineation.

Mylonite samples were collected from six sites along the shear zone with 13–54 specimens from each site (Fig. 1; Table 1). Cylindrical specimens were drilled with a diamond drill-bit, of 2.54 cm

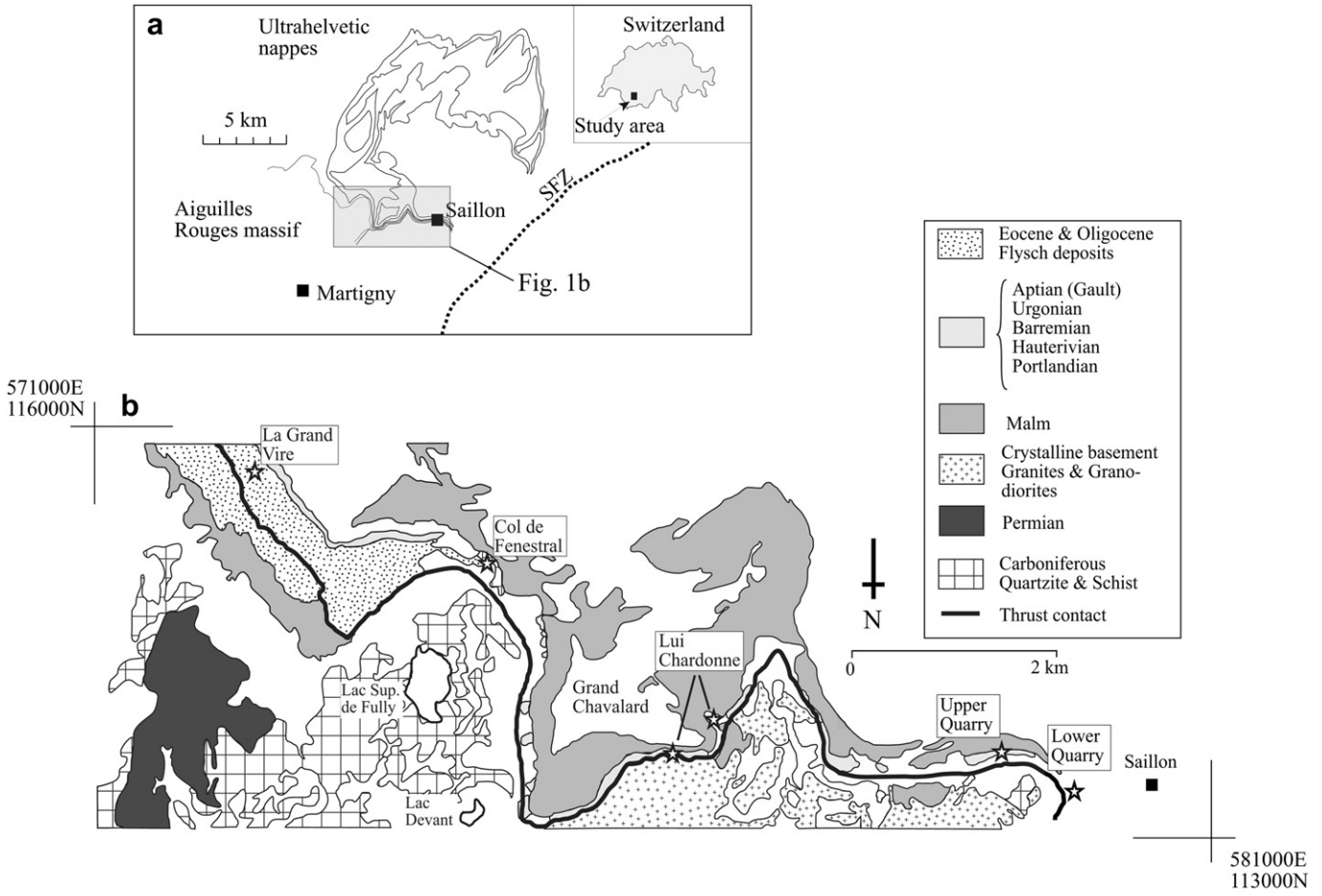

Fig. 1. Map showing the sampling locations along the Morcles nappe shear zone. Note that the site referred to as Martigny in subsequent figures has been displaced by the Rhône–Simplon fault and is located about 11 km southwest of Saillon. The original position of the site at Martigny, prior to displacement, was near the Lower Quarry to the east; the sample site at Martigny experienced highest peak metamorphic conditions. The location of Martigny and the Simplon fault zone (SFZ) are indicated in the inset map (Fig. 1a).

Table 1
Summary of the structural data and sampled lithologies for the different sample locations along the shear zone.

Location	UTM	Average Strike/ Dip of Foliation	Sampled Lithologies
Martigny		131/78[a]	Urgonian, Gault
Lower Quarry	E579650 N113250	130/69	Urgonian, Gault
Upper Quarry	E578650 N113500	112/33	Urgonian
Lui Chardonne	E576200 N113800	127/38	
	E575500 N113500		Urgonian, Malm, Hauterivian, Portlandian
Col de Fenestral	E574050 N115200	108/38	Urgonian
La Grand Vire	E571500 N116500		Urgonian, Gault

[a] The orientation of foliation may not be in situ, because the geologic relationship of the outcrop with respect to the nappe structure is unclear.

diameter and 2.2 cm length, from either oriented block samples in the laboratory or using a portable gasoline-driven drill in the field. Block samples were oriented in the field marking the dip and direction of dip of a planar surface, and oriented cores were drilled normal to this surface. Data obtained from cores drilled from block samples could accordingly be re-oriented to their geographic orientation. The only locality at which in situ samples were not acquired was at La Grand Vire, which is located at the least deformed end of the shear zone close to the frontal folds of the nappe structure. At this site hand samples were collected from loose blocks near outcrops, and cores were oriented with respect to the foliation plane and the stretching lineation observed in the blocks. The locality Lower Quarry displays a secondary tectonic overprint due to a late phase deformation related to displacement along the Rhône-Simplon Fault Zone (Dietrich and Durney, 1986; Seward and Mancktelow, 1994; Ebert et al., 2007). A secondary NE–SW stretching lineation associated with development of open folding of S_1 is found in addition to the main foliation at this site, which is related to the extension parallel to the Alpine Orogen (Fig. 2a,b). Directions of extensional fibres in pressure shadows are related to the NE–SW lineation as observed in the root zone of the nappe stack (Durney and Ramsay, 1973; Casey et al., 1983). Almqvist et al. (2009: *cf.* Fig. 2b) showed two foliations (S_1 and S_2) in a petrographic thin section image from the Lower Quarry. The locality at Lui Chardonne may have also undergone secondary deformation, as seen from local gentle folding of the bedding/cleavage planes at the outcrop.

Most samples were taken from the Urgonian Formation, where calcite is the matrix mineral and second-phase minerals (mainly mica) contribute up to 12 vol% of the total composition, but usually is $<<$10 vol%. The underlying Gault Formation was sampled at three of the sites (Table 1). The Gault Formation consists of calcite with additional mica, quartz, and dolomite as secondary phases in concentrations up to 30 vol% (Ebert et al., 2007). At Lui Chardonne the stratigraphically older Malm, Barremian and Portlandian units were sampled, which can contain up to 40 vol% secondary phases in the case of the Malm (Table 1; Ebert et al., 2007). The calcite contains Fe^{2+} substituting for Ca^{2+}, but in concentrations generally below 1000 ppm. The paramagnetic secondary phases include muscovite, illite and chlorite. Small amounts of diamagnetic quartz and dolomite are present in the Gault and Malm units. Iron-oxides and iron-sulphides are present generally in trace amounts ($<<$1 vol%).

2. Methods

AMS is mathematically described by a second rank symmetrical tensor and can be described by an ellipsoid. The eigenvalues of this tensor represent the principal axes, in which $k_1 \geq k_2 \geq k_3$. The degree of anisotropy in low-field measurements is expressed by Pj (Jelinek, 1981). For high-field magnetic torque measurements, the degree of anisotropy is expressed by the susceptibility difference, $\Delta k = k_1 - k_3$. Technically, the latter is needed to illustrate the anisotropy for high-field torque measurements, since this method measures the deviatoric magnetic susceptibility (Jelinek, 1985). The shape of the susceptibility ellipsoid is given by $U = [(2k_2 - k_1 - k_3)/(k_1 - k_3)]$, where $0 < U \leq 1$ is oblate and $0 > U \geq -1$ is prolate. When $U = 1$, or $U = -1$, the susceptibility ellipsoid is rotational oblate and prolate, respectively (Jelinek, 1981). The bulk magnetic susceptibility (k) is defined as the arithmetic mean of k_1, k_2 and k_3. Diamagnetic minerals and specimens pose a difficulty in the definition of their principal axes (Hrouda, 2004). In this study, because calcite is the dominant diamagnetic mineral, the principal axes of calcite are defined as $k_1 = k_2 = -1.17 \times 10^{-5}$ and $k_3 = -1.28 \times 10^{-5}$ SI, resulting in $U = 1$ for a calcite single crystal, i.e., oblate susceptibility ellipsoid.

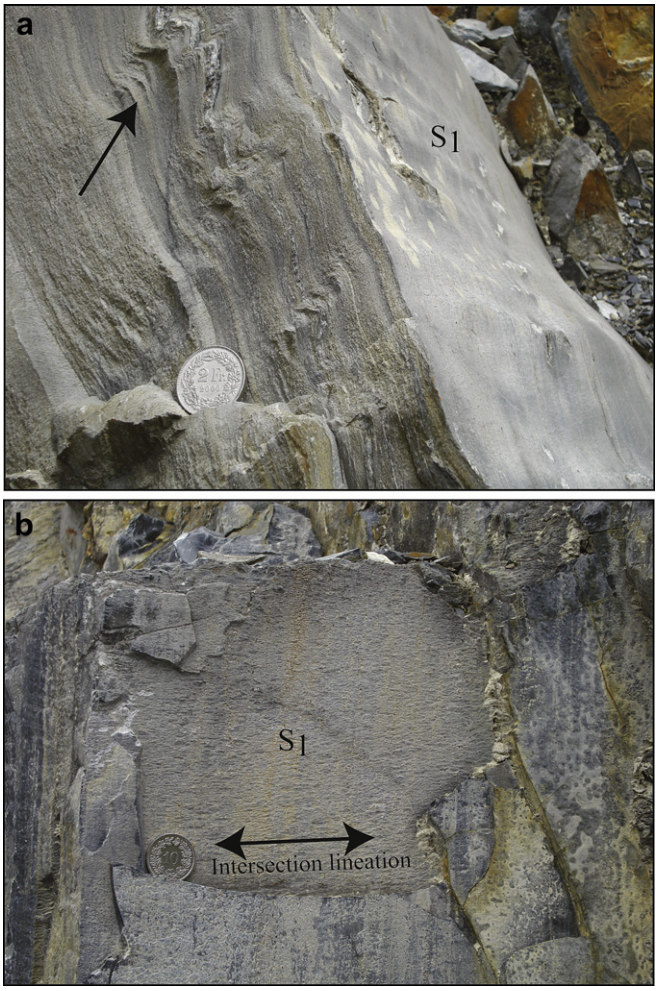

Fig. 2. Outcrop photographs from the Lower Quarry illustrating (a) the primary tectonic foliation plane (S_1), and open folding of the S_1 foliation plane as indicated by the arrow; (b) the intersection lineation (arrow) as seen on the surface of S_1.

Low-field AMS was measured with a KLY-2 (LNM, ETH-Zürich), KLY-3 (Department of Physics, Universidad Complutense de Madrid), and KLY-4 (Institute for Applied Geosciences, Karlsruhe Institute of Technology) AGICO Kappabridge, using a 300 A/m alternating field with 875 Hz frequency. High-field measurements were performed with a torque magnetometer (Bergmüller et al., 1994) at room temperature and 77 K, in six fields ranging from 700 to 1500 mT, plus in the absence of an applied field (zero field). The signal due to the holder and zero field measurements were subtracted from the total torque. At room temperature the high-field measurements enables

separation of the anisotropy that is due to ferrimagnetic grains (Martín-Hernández and Hirt, 2001). Measurements at 77 K are used for the separation of the paramagnetic and diamagnetic anisotropies, by the method outlined in Schmidt et al. (2007a), which is briefly introduced as follows.

The magnetic susceptibility of paramagnetic minerals obey the Curie–Weiss law, which is defined as

$$k_p = \frac{C}{T - \theta} \quad (1)$$

where C is the Curie constant, θ is the paramagnetic Curie temperature and T is the absolute temperature. The bulk susceptibility of a paramagnetic mineral is ~3.8 times higher at 77 K compared to room temperature conditions (293 K) under the assumption that θ ~ 0 K. The paramagnetic anisotropy at 77 K has to be determined specifically for each mineral species. To describe the change in anisotropy from room temperature to 77 K a ratio of the paramagnetic susceptibility difference (Δk^{para}) at 77 K to the Δk^{para} at 293 K is used, which is called the p77-factor. The p77-factor for several carbonate minerals and muscovite was determined experimentally by Schmidt et al. (2007a, 2007b, 2009). For iron-rich calcite, in the range of 500 ppm to 11,000 ppm Fe, p77 = 13.3 (Schmidt et al., 2007b) and for muscovite mica p77 = 8.23 (Schmidt et al., 2007a, 2009). For the purpose of subfabric separation in this study the latter value was used for sheet-silicate rich specimens (e.g., Gault), whereas the former value was used for the nearly pure calcites (e.g., Urgonian).

Calcite texture measurements were made on selected samples from the shear zone using electron backscatter diffraction (EBSD) and X-ray diffraction (XRD) texture goniometry. Measurements

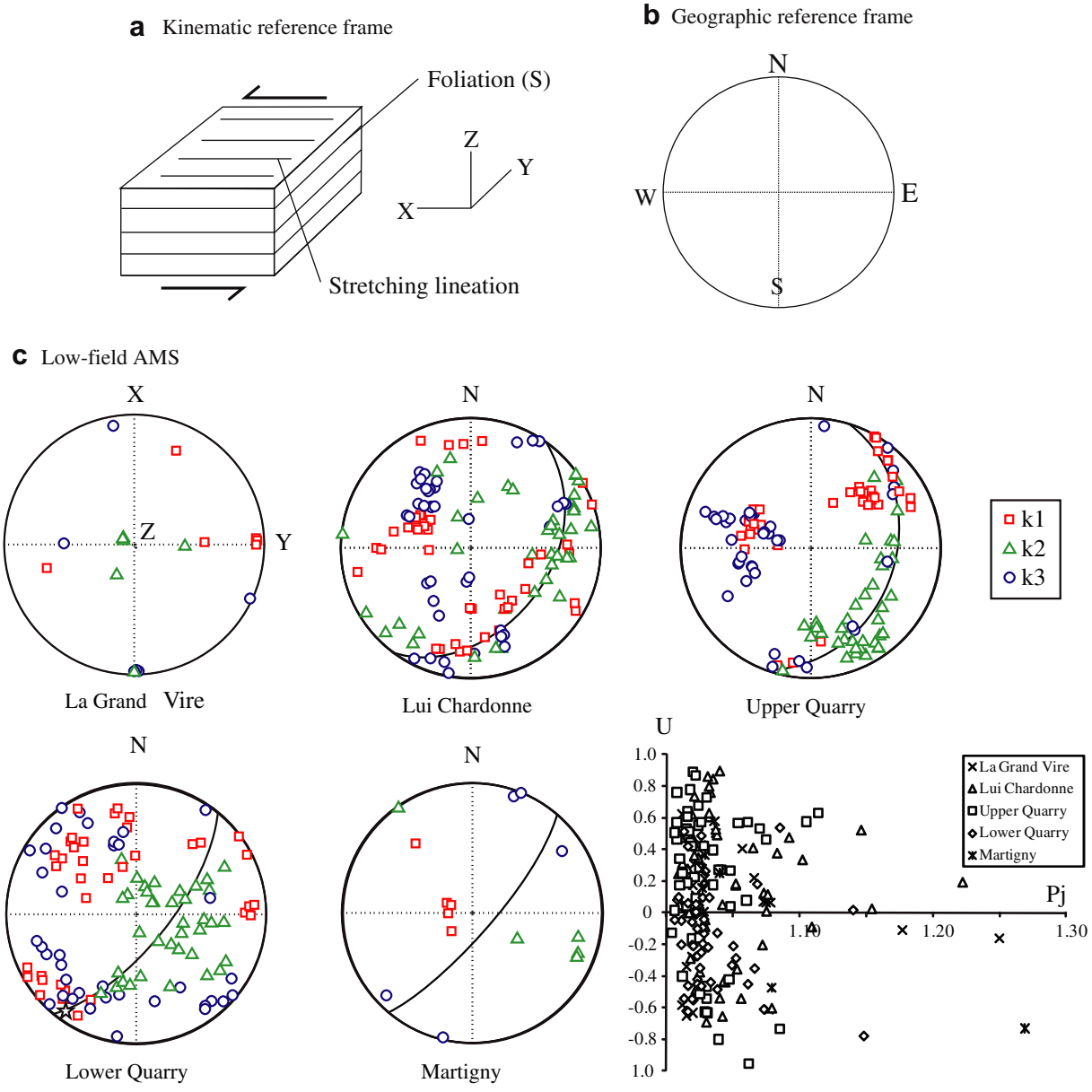

Fig. 3. Equal area projections showing the orientation for axes of principal magnetic susceptibility measured in low-field for the different sample sites; squares represent the maximum susceptibility (k_1); triangles show the intermediate susceptibility axis (k_2); circles show the minimum susceptibility axis (k_3), in this and subsequent figures. The orientation of the primary foliation plane is shown by the great circle; the star indicates the axis of the intersection lineation observed in the Lower Quarry. The degree of susceptibility (Pj) and shape parameter (U) calculated from the low-field measurements are shown in the lower right plot. AMS for all sample locations are shown in geographic coordinates, with the exception of La Grand Vire where block samples were not oriented in situ, but relative to the stretching lineation (X) and the pole to the foliation plane (Z).

Table 2
F-distribution test (comparison of variances) at 95% confidence interval, with [2, 9] degrees of freedom.

Location	n	Within 26° Cone of 95% ca	Outside 26° Cone of 95% ca	% Anisotropic Specimens
La Grand Vire	25	6	21	24
Col de Fenestral	15	0	15	0
Lui Chardonne	46	40	6	87
Upper Quarry	54	38	16	70
Lower Quarry	53	37	16	70
Martigny	13	6	7	46

n - number of specimens.

were done on the polished core-ends of the AMS specimens, such that EBSD/XRD and AMS were measured on the same specimens. The details of the EBSD experimental procedure are outlined in Almqvist et al. (2010). XRD goniometry measurements were performed at the University of Göttingen, using a PANalytical X-ray diffractometer (X'pert PRO MRD, PW3040; Leiss, 2005; Leiss and Ullemeyer, 2006) with an attached polycapillary at the primary beam side. This results in parallel beam optics with high resolution in d-spacing even at large tilting angles and a large beam size of 7 mm. For the pole figure measurements of (006) (012) (110) (104) (113) and (202), a grid spacing of 5° × 5° was applied. A 1 s exposure time at each grid-point was used, with X-ray beam operating conditions of 40 kV and 40 mA.

Due to the defocusing effect (*cf.* Kocks et al., 1998), pole figures are incomplete – in our case at tilt angles >70°. A quantitative texture analysis was carried out by means of the orientation distribution function (ODF) by applying the WIMW routine (BEARTEX software, Wenk et al., 1998). Using the ODF for calcite the theoretical diamagnetic AMS was calculated, using a petrophysical software package (Unicef Careware; Mainprice, 1990).

3. Results

3.1. Low-field AMS

The magnetic fabric, measured in low fields (LF-AMS), is controlled in general by the foliation, which is related to the thrusting taking place along the shear zone (Fig. 3). La Grand Vire and Col de Fenestral, which are located in the distal part of the shear zone, display a very weak magnetic fabric with a loose grouping of k_3–axes as pole to S_1 (Fig. 3). The weak anisotropy is emphasised by the large number of specimens that fail the anisotropic f-test (at 95% confidence limit) at these location (Table 2; Jelinek, 1976). Failure of the f-test is defined by individual specimens having confidence angles ≥26° for at least two of the three principal axes. Table 2 lists the number of specimens that have been rejected, after failing the f-test; rejection indicates that the specimen is isotropic. All samples at Col de Fenestral, which were measured on a KLY-2 Kappabridge were isotropic (this may in part be due to the less sensitive measurements of the KLY-2). The number of specimens that fail the f-test at the other sites range from 13 to 84%. Isotropic specimens have a bulk susceptibility close to -10×10^{-6} SI, which is in the range where the paramagnetic and diamagnetic anisotropies cancel one another (Almqvist et al., 2010).

An inverse magnetic fabric is found in specimens that have $-10 \times 10^{-6} < k < 0$ SI (i.e., k_1 as the pole to the cleavage), indicating that the paramagnetic anisotropy of iron is responsible for the orientation of the principal axes. When the bulk susceptibility is higher than $10–20 \times 10^{-6}$ SI the magnetic fabric is typically normal, with k_3 subparallel to the pole to cleavage, indicating that phyllosilicates are responsible for the magnetic fabric. A second fabric, however, is seen at the Lower Quarry locality, with clustering of k_1- and k_3-axes oriented shallow and NE–SW, clustering about the stretching lineation observed at this location (Fig. 3).

The degree of anisotropy (Pj) varies from close to 1.0 up to 1.3. Some samples with extreme degree of anisotropy (Pj > 4) have been removed from the plot in Fig. 3, since their high values originate from the bulk susceptibility having values near zero (Hrouda, 1986, 2004). The susceptibility ellipsoids display shapes ranging from nearly rotational oblate to nearly rotational prolate, with large variation between these two extremes.

3.2. High-field AMS

High-field AMS (HF-AMS) was measured for selected specimens at room temperature and 77 K. The magnetic torque increases as the square of the applied field for all specimens. Examples from the Urgonian and Gault units are shown in Fig. 4 (a, b). The ferrimagnetic contribution to the torque is negligible in both cases, as indicated by the regression lines intersecting close to the origin. Comparatively, the torque at room temperature for the Gault is

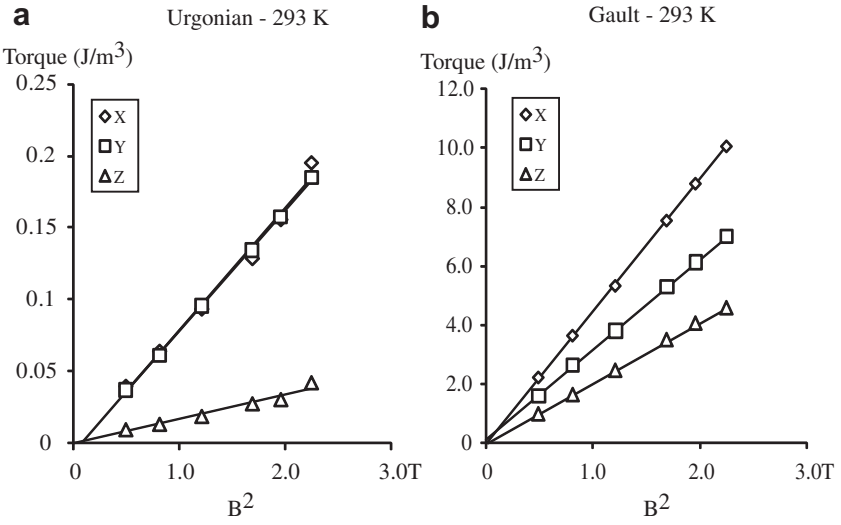

Fig. 4. The magnetic torque as a function of the square of the applied field (B^2) for three orthogonal sample positions. The sample reference frame referred to in the legend is the same as presented in Fig. 3.

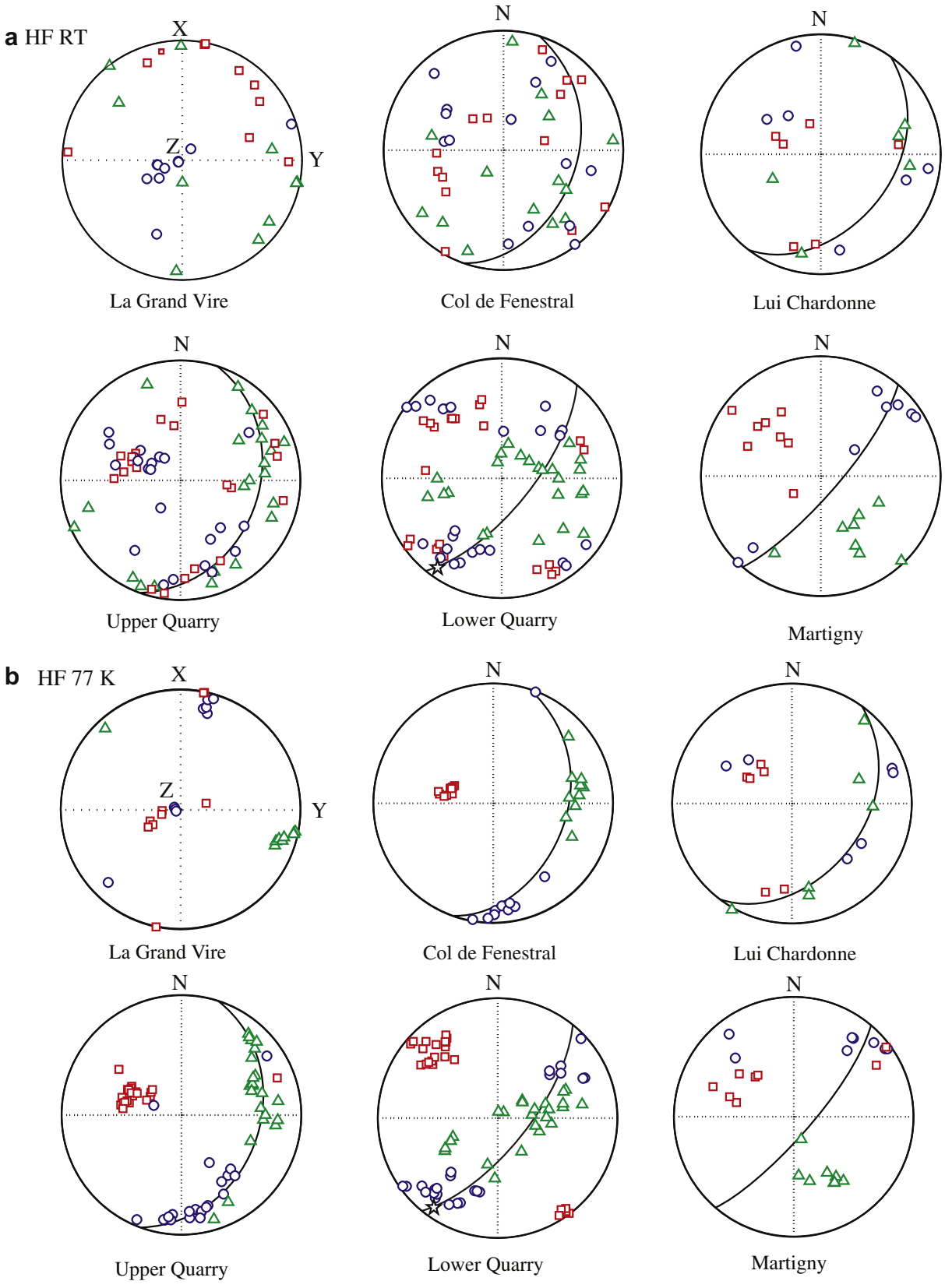

Fig. 5. Equal area projections showing the principal axes of susceptibility measured with the high-field torque magnetometer at (a) room temperature and (b) 77 K.

nearly 50 times larger than for the Urgonian, due to the high concentration of paramagnetic minerals in the former specimen.

Fig. 5a shows the non-ferrimagnetic anisotropy at room temperature, which arises from the sum of paramagnetic and diamagnetic subfabrics. The orientation of the principal axes of the HF-AMS at room temperature is similar to the LF-AMS. All sites display a magnetic fabric that is largely dominated by flattening, and development of S_1. The Lower Quarry and Martigny additionally show indication of the subsequent deformation. The shapes of the susceptibility ellipsoids range from oblate to prolate, and have low susceptibility differences (Fig. 6a). There is a trend of oblate ellipsoid with low susceptibility differences to prolate ellipsoids with increasing degree of anisotropy (Δk).

The HF-AMS at 77 K have higher degree of anisotropy, one to two orders of magnitude larger, than the room temperature anisotropy (Fig. 6b). In addition, the distribution of principal axes are better constrained at 77 K (Fig. 5b), especially for specimens that were weakly anisotropic at room temperature. Most ellipsoids have prolate shape (Fig. 6b), which suggest the enhancement and an inverse fabric, i.e., k_1 close to the pole to foliation, of the anisotropy originating from iron-rich calcite, except in the case of the Lower Quarry where the average ellipsoid is nearly neutral.

Using the low temperature measurements the paramagnetic and diamagnetic subfabrics have been separated, resulting in a distinct difference between the diamagnetic and paramagnetic anisotropy (Fig. 6a, b and 7a, b). This is seen primarily by principal axes oriented sub-parallel to the pole to cleavage; for the paramagnetic sub-fabric it is the k_1-axes, whereas it is the k_3-axes for the diamagnetic fabric. The only exception is at Lui Chardonne, where k_1-axes orient sub-parallel to the S_1 pole for the diamagnetic fabric; this will be further discussed below. The paramagnetic fabric is dominantly prolate, with the exception of the Lower Quarry and to a lesser extent Lui Chardonne (Fig. 6c). This departure is related to the later stage deformation and is also discussed below. There is a trend to increasing degree of anisotropy along the shear zone. The separated diamagnetic fabrics fall predominantly in the oblate field, again with exceptions from the Lower Quarry and Lui Chardonne (Fig. 6d). In the case of the diamagnetic anisotropy, the values of Δk range between $\sim 1.0 \times 10^{-7}$ and $\sim 9.0 \times 10^{-7}$ SI, which is well below the single crystal value for calcite (1.10×10^{-6} SI). The highest values for Δk are observed from Martigny, the Upper Quarry and the Lower Quarry, in contrast to low values at La Grand Vire in the distal portion of the shear zone. As the degree of alignment of the calcite crystals increase, Δk will approach the value for a single crystal of calcite. Note that the Δk of a single crystal is only hypothetically achievable for a monomineralic rock when all crystals are perfectly aligned, i.e., reaches saturation alignment and the texture strength (J-index) is infinitely large (Borradaile and Jackson, 2010).

We have calculated the theoretical AMS based on the calcite texture, which was measured using EBSD and XRD goniometry. The calcite AMS is calculated based on the single crystal magnetic susceptibility tensor for calcite (Schmidt et al., 2006) and the crystallographic preferred orientation (CPO), using the software of Mainprice (1990). Results for the predicted AMS due to calcite are compared with the separated diamagnetic anisotropy in Fig. 8, where in general the calculated and measured Δk and U show very good correlation. The separation is not successful for some

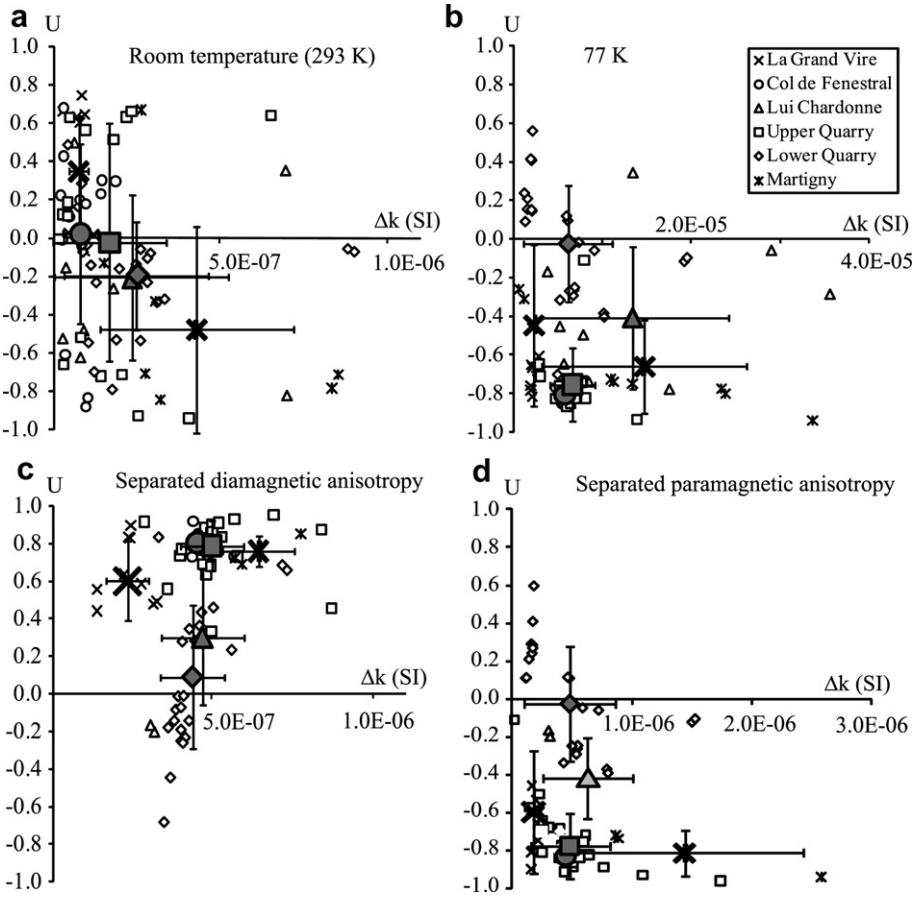

Fig. 6. Shape parameter (U) against the susceptibility difference (Δk) for high-field measurements made at (a) room temperature and (b) 77 K, as well as for the separated (c) diamagnetic and (d) paramagnetic anisotropy. Large symbols indicate the site mean, with corresponding error bars for 1σ confidence.

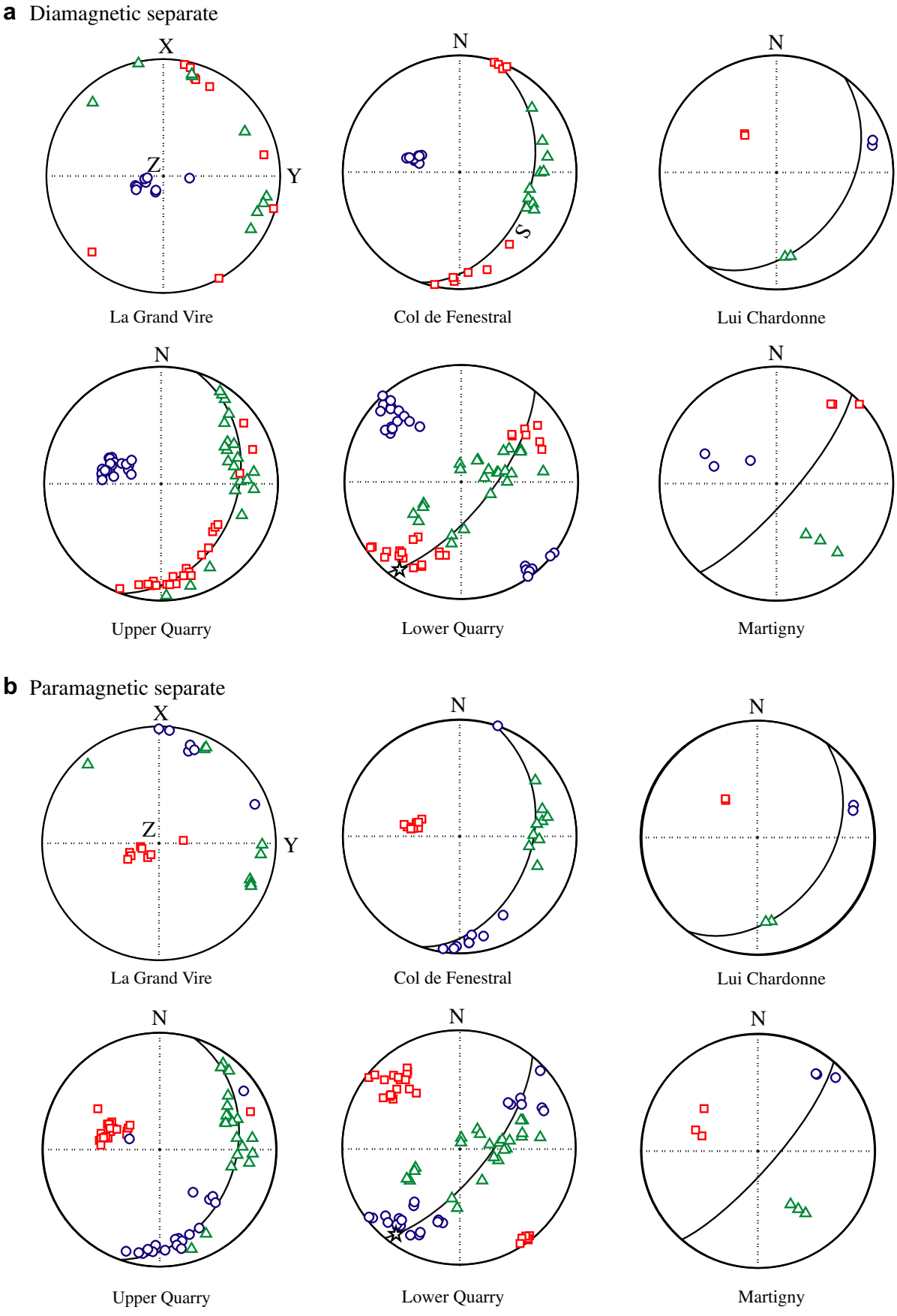

Fig. 7. Equal area nets illustrating the principal susceptibility axes for the separated (a) diamagnetic and (b) paramagnetic anisotropy.

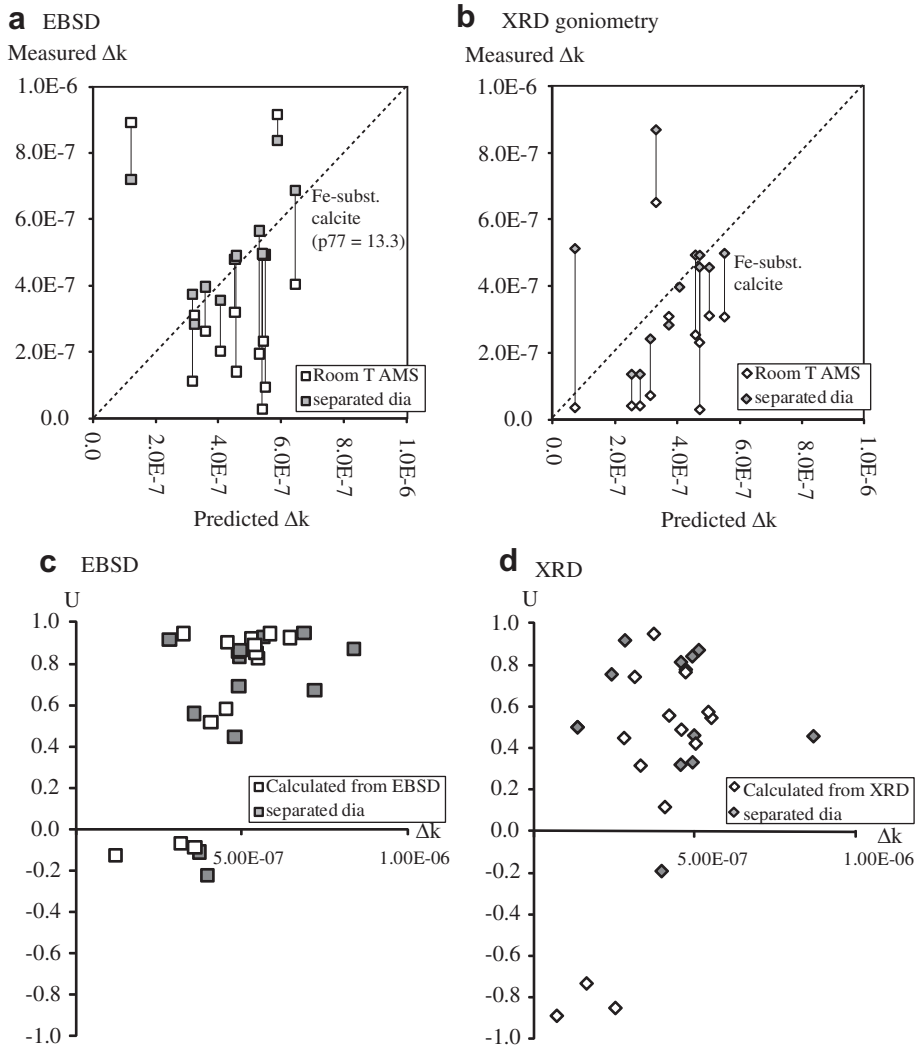

Fig. 8. (a) and (b) illustrate the susceptibility difference of the separated diamagnetic anisotropy and the calculated magnetic anisotropy for calcite, where the latter is based on EBSD and XRD CPO measurements and the single-crystal AMS tensor of calcite (Schmidt et al., 2006); (c) and (d) Δk and U shown for the separated diamagnetic anisotropy and calculated based on the calcite CPO.

specimens, shown by the poor agreement between measured and predicted Δk. Two explanations for this can be invoked, 1) the p77-factor used for iron-rich calcite is inappropriate in these cases, or 2) the calculated Δk is misleading due to errors originating from the texture measurements. Given that both the EBSD and XRD display outliers, it seems likely that the chosen p77-factor is incorrect, i.e. that iron-rich calcite is not solely responsible for the paramagnetic sub-fabric.

4. Discussion

Deformed carbonates from the shear zone demonstrate the importance of being able to separate magnetic subfabrics in a multi-phase rock made up of either a mix of paramagnetic and diamagnetic minerals, or a single diamagnetic phase containing paramagnetic elements in its crystal lattice. Due to the difference in sign of the susceptibility a paramagnetic anisotropy can work against the diamagnetic anisotropy, which can be the case when the two subfabrics are co-axial. The LF-AMS can appear to be isotropic, although the individual paramagnetic and diamagnetic subfabrics are significantly anisotropic, and in the worst case can lead to erroneous interpretations in a geologic context. Low temperature measurements in either low-field or high-field enhances the susceptibility and anisotropy of paramagnetic minerals (e.g., Ihmlé et al., 1989; Hirt and Gehring, 1991; Richter and van der Pluijm, 1994; Lüneberg et al., 1999; Parés and van der Pluijm, 2002; Martín-Hernández et al., 2005; Debacker et al., 2009). Measurements performed at 77 K provide an advantage when the Δk at room temperature is low and the bulk susceptibility is ~0 SI, since the diamagnetic and paramagnetic contribution to the bulk susceptibility are close to equal at room temperature, but very different at 77 K. The effectiveness of measuring at low temperature is shown by the similar fabrics obtained for HF-AMS at 77 K and the separated paramagnetic fabric (Figs. 5b and 7b). Measurements in high fields at room and low temperature allow the isolation of the paramagnetic and diamagnetic subfabrics.

At room temperature the LF-AMS and HF-AMS display significant scatter in the orientation of principal axes, resulting from the weak degree of anisotropy due to the competition between the paramagnetic and diamagnetic subfabrics (e.g., Almqvist et al., 2010). HF-AMS at 77 K produces a better grouping of principal axes, which is largely due to the enhancement of the paramagnetic susceptibility. The inverse fabric indicates that the paramagnetic anisotropy arises from the presence of Fe^{2+} in the calcite structure (Rochette, 1988; Ihmlé et al., 1989). Paramagnetic second phases such as mica have minor influence on the AMS, with the exception

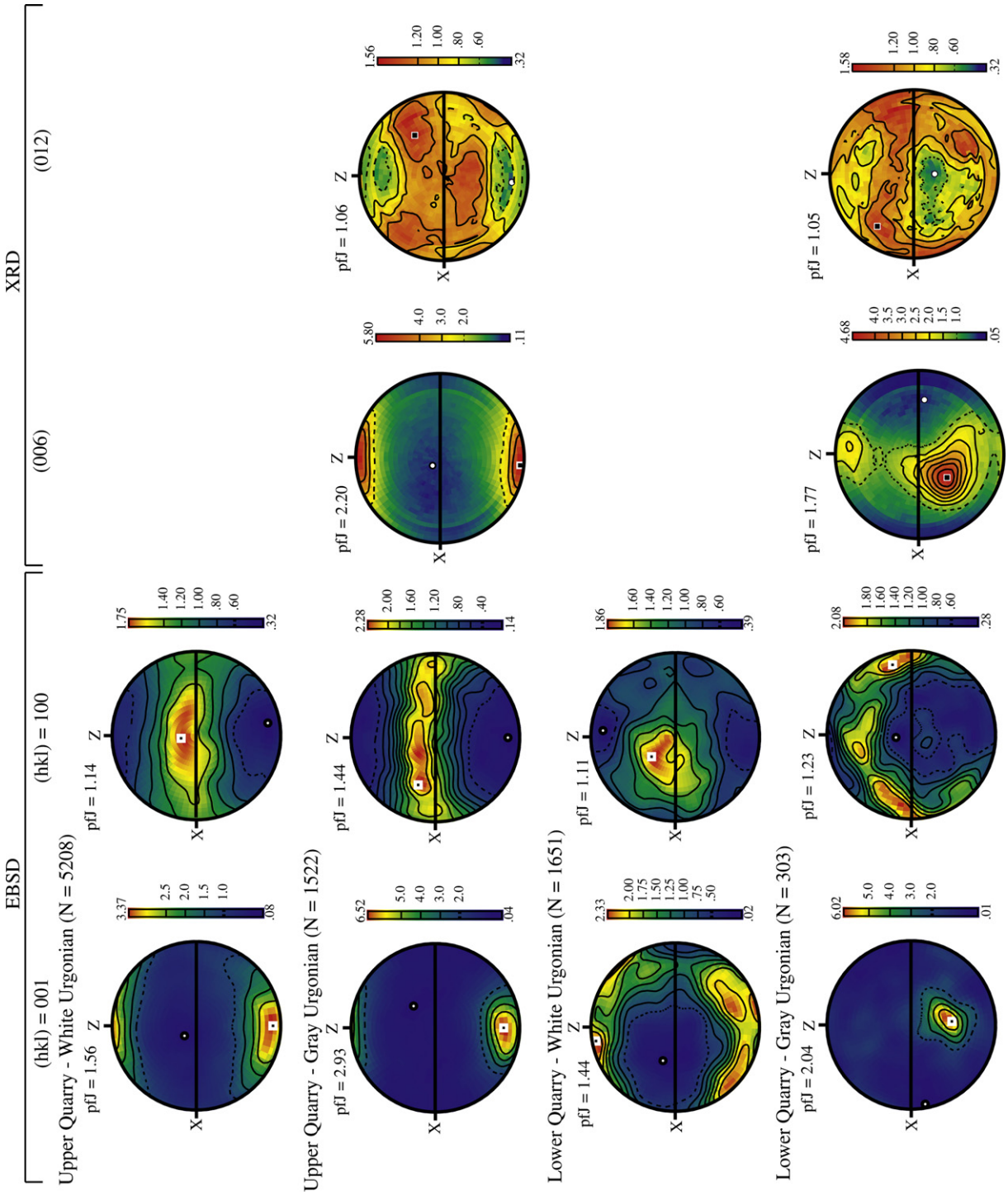

Fig. 9. A series of calcite pole figures from White and Grey Urgonian specimens at the Lower and Upper Quarry, which display *a*- crystallographic axes concentrations (100) and the *c*-axes (001) concentrations, measured with EBSD (left), and the (006) and (012) pole figures from XRD goniometry measurements. Contours are multiples of uniform distribution (MUDs), with an inverse log colour scale; circles represent minimum concentration of *a*- or *c*-axes or poles to planes; squares are the maximum concentration of *a*- and *c*-axes or poles to planes; Pfj is the pole figure J-index. N is the number of EBSD data acquired for each specimen. Pole figure data are plotted on lower hemisphere equal area nets, where X represents the orientation of the structural foliation plane and Z is the pole to the foliation plane (see Fig. 3a for the kinematic reference frame). Note that the pole figures shown represent EBSD and XRD measurements performed on specimens from the same rock sample, but not the same specimen.

for samples with a bulk susceptibility higher than 1.0×10^{-5} SI (N.B., the majority of samples collected from the shear zone records negative bulk susceptibility).

Near prolate shape of the susceptibility ellipsoids at 77 K further indicate that the paramagnetic anisotropy originate from the Fe-substitution in calcite for the majority of specimens. Earlier work from the Morcles nappe showed that either k_3 will be sub-parallel to the pole to the foliation in the case of iron-poor calcite (<400 ppm Fe^{2+}; normal magnetic fabric), or k_1 is sub-parallel to the pole to foliation in iron-rich calcite (>400 ppm Fe^{2+}, an inverted magnetic fabric; Ihmlé et al., 1989; Almqvist et al., 2009, 2010).

Success in separating the diamagnetic fabric is dependent on having an accurate value for the p77-factor (Schmidt et al., 2007a). This requires knowledge of the paramagnetic phase or source responsible for its sub-fabric; otherwise the characteristics of the separated anisotropy will be false. In general for samples from the Morcles nappe the p77-factor for iron-rich calcite is suitable for samples, judging from the comparison between measured and predicted calcite AMS (Fig. 8). One exception is at Lui Chardonne where the diamagnetic sub-fabric is inverse. The appropriate p77 value has not been determined for samples from this location.

Flattening, due to high shear strain (e.g., Ramsay et al., 1983), is the main factor controlling the LF-AMS and HF-AMS along the basal shear zone of the Morcles nappe. The AMS results from the different sample locations are consistent with interpretation of the regional deformation events, in which shear movement took place in a northwesterly direction (Dietrich, 1986; Dietrich and Song, 1984; Ebert et al., 2007). Orientations of the principal axes for the paramagnetic and diamagnetic subfabrics are consistent with the main deformation on the inverted limb, with the exception of the Lower Quarry. The degree of anisotropy reflects the strain gradient along the length of the shear zone, with the most intense deformation taking place in the root of the nappe structure. Whereas brittle processes are typical in the front of the nappe, simple shear is important in the more internal parts of the shear zone where plastic deformation processes operate (Ebert et al., 2007; Austin et al., 2008).

The tectonic overprint identified in the Lower Quarry is also evident from the texture, as shown by *c*- and *a*-axes calcite pole figures measured with EBSD, and in the (006) and (012) pole figures measured by XRD goniometry (Fig. 9). For a White Urgonian sample, collected from the Lower Quarry the concentration of *a*-axes are located at an oblique angle to the main foliation (S_1), and *c*-axes are offset with respect to the pole to S_1, and have a tendency to be distributed in a girdle rather than a point maximum. Note that EBSD and XRD goniometry pole figures presented in Fig. 9 were made on specimens from the same rock sample, but not on the same specimens (i.e., a bulk sample of a about 100 cm^3 volume). The *a*-axes for a Grey Urgonian sample from the Lower Quarry are oriented in a girdle, but the distribution is oblique with respect to S_1. The overprint related to the late phase deformation is not readily observed in pole figure of samples from the Upper Quarry, and *a*- and *c*-axes appear normally distributed with respect to S_1, i.e., a girdle of *a*-axes sub-parallel to S_1 and the *c*-axis maximum as the pole to S_1. In general the texture intensity (J-index and MUDs) is weaker in calcite pole figures from the Lower Quarry, compared to the Upper Quarry, which corresponds to observations of lower average degree of anisotropy (Δk) in the Lower Quarry. A stronger overprint in the Lower Quarry is inferred from the differences observed in pole figures from each location. The relatively weaker texture strength observed in the XRD goniometry pole figures is thought to arise from 1) the lack of complete pole figures, and 2) the larger volume considered in X-ray measurements compared to EBSD measurements, which likely reduces the CPO intensity. Although the texture strength is somewhat weaker in the XRD goniometry pole figures, there is general coincidence of the CPO when comparing the two methods.

The microstructures of calcite provide another indicator for the partial overprint in the Lower Quarry (Ebert, 2006). Standard deviation of the grain-size of calcite is higher for specimens in the Lower Quarry, whereas the mean grain-size is similar at the Lower and Upper Quarries. The grain-size skewness and kurtosis have considerably higher positive values for samples in the Lower Quarry. The differences in grain-size characteristics in the Lower Quarry hints at different deformation conditions, although a more in depth analysis of microstructures is beyond the scope of this work.

The development of the main tectonic foliation (S_1) and partial overprint is reflected in the diamagnetic sub-fabric (Fig. 10). An increase in the degree of anisotropy (Δk) is related to increasing strain towards the root of the nappe, going from the least deformed location at La Grand Vire, to the highly deformed Upper and Lower Quarry, in accordance with the temperature gradient and increasing strain along the shear zone. This is illustrated by the arrow in Fig. 10 that is accompanied by the number one. Partial overprinting associated with the Rhône–Simplon fault yield a composite magnetic fabric, observed in the Lower Quarry and at Lui Chardonne (2). Therefore, overprinting with a second tectonic flattening results in a decrease in the degree of anisotropy; this is accompanied by a change of shape of the susceptibility ellipsoid towards prolate (Fig. 10, arrow marked with the number two). This is similar to what Kligfield et al. (1981, 1983) and Siddans et al. (1984) showed in the Alps Maritimes, where an initial sedimentary bedding compaction is overprinted by subsequent tectonic flattening. But in contrast to the Alps Maritimes, the composite magnetic anisotropy in the Morcles nappe originates from two successive tectonic flattening events. In this sense, magnetic anisotropy can be useful to unravel peak metamorphic deformation structures from the corresponding structures that evolve during retrograde deformation. Changes in Δk and U reflect weakening of the CPO, which itself results from reduced temperature during partial overprinting.

The NE–SW stretching lineation, and corresponding magnetic fabric, is related to tectonic movement parallel to the general trend of the Central Alps (i.e., Steck, 1984; Steck and Hunziker, 1994). Mancktelow (1985, 1990, 1992) observed the development of NE–SW stretching lineation in relation to plastic deformation along the footwall of the Rhône–Simplon fault. Backfolding took place during the

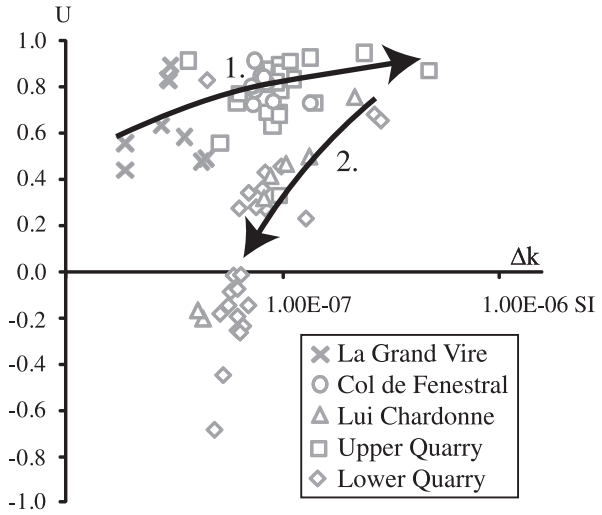

Fig. 10. U as a function of Δk for the separated diamagnetic sub-fabric at the different locations along the Morcles nappe shear zone. Arrows accompanied by the numbers are addressed in the text.

upper Miocene with related NW–SE shortening near the Simplon Pass (Mancktelow, 1992), which penetrated the root zone of the entire nappe stack. Parts of the Morcles root zone were displaced by the dextral western continuation of the Rhône–Simplon line (Burkhard, 1988; Soom, 1990; Mancktelow, 1990, 1992; Steck and Hunziker, 1994; Seward and Mancktelow, 1994; Ebert et al., 2007).

Partial overprinting due to orogen parallel extension also appears to take place at Lui Chardonne and possibly at the Upper Quarry, as seen in the Jelinek diagram for the separated diamagnetic sub-fabric (Fig. 10), where a decreasing susceptibility difference is coupled with susceptibility ellipsoids that move towards and into the prolate field. Although the overprint is weak, this suggests that large parts of the Morcles fold is affected, and overprinting is not limited to the local vicinity of Rhône-Simplon line.

5. Conclusions

Anisotropy of magnetic susceptibility has been used to study deformed calcite mylonites from the Morcles nappe shear zone. Low- and high-field AMS measurements at room temperature show a composite magnetic fabric with broad scatter due to the weak susceptibility of the rocks. These measurements produce results that display mixed inverse and normal magnetic fabrics for samples collected from the same location, which arise from the coupled contribution of paramagnetic and diamagnetic minerals. The isolated diamagnetic and paramagnetic subfabrics coincide with the intensity of the calcite texture, which was determined from electron backscatter diffraction and X-ray texture goniometry measurements. Magnetic subfabrics are consistent with the deformation history of the Morcles Nappe and indicate that 1) there is a strain gradient along the shear zone, and 2) in addition to the original tectonic imprint that arose during NW transport of the nappe stack, a prominent NE–SW stretching is evident in several locations along the shear zone that originates from subsequent tectonic overprinting. These results highlight that secondary deformation due to orogen parallel extension is not be limited to the Rhône Valley floor, but also occur locally at higher levels in the nappe stack.

Acknowledgements

This work was supported by the Swiss National Science Foundation, project 2-77070-07. We thank Graham Borradaile and Bernard Henry for constructive reviews, whose comments and suggestions improved the manuscript. The authors wish to thank Jens M. Walter for assistance with X-ray diffraction goniometer measurements in Göttingen. Belén Oliva-Urcia, Agnes Kontny and Fátima Martín-Hernández assisted with laboratory measurements in Karlsruhe and Madrid. The software used to illustrate the calcite pole figures was developed by David Mainprice. This work benefitted from discussions with Neil Mancktelow. Øyvind Paasche, Claudio D'addario and Jessica Kind assisted during field work.

References

Almqvist, B.S.G., Hirt, A.M., Schmidt, V., Dietrich, D., 2009. Magnetic fabrics of the Morcles Nappe complex. Tectonophysics 466, 89–100.

Almqvist, B.S.G., Herwegh, M., Schmidt, V., Pettke, T., Hirt, A.M., 2010. Magnetic susceptibility as a tool to study deformed calcite with variable impurity content. Geochemistry, Geophysics, Geosystems 11. doi:10.1029/2009GC002900.

Austin, N., Evans, B., Herwegh, M., Ebert, A., 2008. Strain localization in the Morcles nappe (Helvetic Alps, Switzerland). Swiss Journal of Geosciences 101, 341–360.

Bergmüller, F., Bärlocher, C., Geyer, B., Grieder, M., Heller, F., Zweifel, P., 1994. A torque magnetometer for measurements of the high-field anisotropy of rocks and crystals. Measurement Science and Technology 5, 1466–1470.

Borradaile, G.J., 1988. Magnetic susceptibility, petrofabrics and strain. Tectonophysics 156, 1–20.

Borradaile, G.J., Hamilton, T.D., 2004. Magnetic fabrics may proxy as neotectonic stress trajectories, Polis Rift, Cyprus. Tectonics 23, TC1001. doi:10.1029/2002TC001434.

Borradaile, G.J., Fralick, P., Lagroix, F., 1999. Acquisition of anhysteretic remanence and tensor subtraction from AMS isolates true palaeocurrent grain alignments. In: Tarling, D.H., Turner, P. (Eds.), Paleomagnetism and Diagenesis in Sediments. Geological Society, London, Special Publications, vol. 151, pp. 139–145.

Borradaile, G.J., Jackson, M., 2010. Structural geology, petrofabrics and magnetic fabrics (AMS, AARM, AIRM). Journal of Structural Geology 32, 1519–1551.

Burkhard, M., 1988. Horizontalschnitt des Helvetikums der Westschweiz auf 2500 m zwischen Mt. Blanc und Aar-Massiv (Rawil-Depression). Geologische Berichte (Bern), 4. Landeshydrologie und geologie; Bundesamt fuer Umweltschutz, Bern, Switzerland, p. 34.

Casey, M., Dietrich, D., Ramsay, J.G., 1983. Methods for determining deformation history for chocolate tablet boudinage with fibrous crystals. Tectonophysics 92, 211–239.

Collet, L.W., 1927. The Structure of the Alps. Arnold, London, p. 289.

Daly, L., Henry, B., 1983. Prospect for numerical information on finite rock strain from the separation of magnetic anisotropy components. Compte Rendus de l'Acadadémie de sciences 296, 153–156. Paris.

deWall, H., Bestmann, M., Ullemeyer, K., 2000. Anisotropy of diamagnetic susceptibility in Tassos marble: a comparison between measured and modeled data. Journal of Structural Geology 22, 1761–1771.

Debacker, T.N., Hirt, A.M., Sintubin, M., Robion, P., 2009. Differences in magnetic and mineral fabrics in low-grade, cleaved siliciclastic pelites: a case study from the Anglo-Brabant deformation belt (Belgium). Tectonophysics 466, 32–46.

Dietrich, D., 1986. Change of direction of overthrust shear in the Helvetic nappes of western Switzerland. Journal of Structural Geology 8, 389–398.

Dietrich, D., Song, H., 1984. Calcite fabrics in a natural shear environment, the Helvetic nappes of western Switzerland. Journal of Structural Geology 6, 19–32.

Dietrich, D., Durney, D.W., 1986. Change of direction of overthrust shear in the Helvetic nappes of western Switzerland. Journal of Structural Geology 8, 389–398.

Durney, D.W., 1972. Deformation history of the Western Helvetic nappes, Valais, Switzerland. Unpublished PhD Thesis, University of London.

Durney, D.W., Ramsay, J.G., 1973. Incremental strains measured by syntectonic crystal growth. In: DeJong, K., Scholten, R. (Eds.), Gravity and tectonics. Wiley, New York, pp. 67–96.

Ebert, 2006. Microfabric evolution in pure and impure carbonate mylonites and their role for strain localization in large-scale shear zones. PhD Thesis, University of Bern, Switzerland.

Ebert, A., Herwegh, M., Evans, B., Pfiffner, A., Austin, N., Vennemann, T., 2007. Microfabrics in carbonate mylonites along a large-scale shear zone (Helvetic Alps). Tectonophysics 444, 1–26.

Goldstein, A.G., 1980. Magnetic susceptibility anisotropy of mylonites from the Lake Char mylonite zone, SE New England. Tectonophysics 66, 197–211.

Goy-Eggenberger, D., 1998. Faible métamorphisms de la nappe de Morcles: minéralogie et géochemie. Unpublished PhD Thesis, Université de Neuchatel, Neuchatel, Switzerland, p. 192.

Hamilton, T.D., Borradaile, G.J., Lagroix, F., 2004. Sub-fabric identification by standardization of AMS: an example of inferred neotectonic structures from Cyprus. In: Martín-Hernández, F., Lüneberg, C.M., Aubourg, C., Jackson, M. (Eds.), Magnetic Fabric: Methods and Applications. Geological Society, London, Special Publications, vol. 238, pp. 527–540.

Henry, B., Daly, L., 1983. From qualitative to quantitative magnetic anisotropy analysis; the prospect of finite strain calibration. Tectonophysics 98, 327–336.

Hirt, A.M., Gehring, A.U., 1991. Thermal alteration of the magnetic mineralogy in ferruginous rocks. Journal of Geophysical Research 96, 9947–9953.

Hirt, A.M., Lowrie, W., Clendenen, W.S., Kligfield, R., 1988. The correlation of magnetic anisotropy with strain in the Chelmsford formation of the Sudbury basin, Ontario. Tectonophysics 145, 177–189.

Hirt, A.M., Julivert, M., Soldevila, J., 2000. Magnetic fabric and deformation in the Navia-Alto Sil slate belt, northwestern Spain. Tectonophysics 320, 1–16.

Hrouda, F., 1979. The strain interpretation of magnetic anisotropy in rocks of the Nizky Jesenik Mountains (Czechoslovakia). Sbornik Geologickych Ved. (Uzit Geofyzika) 16, 27–62.

Hrouda, F., 1986. The effect of quartz on the magnetic anisotropy of quartzite. Studia Geophysica et Geodaetica 30, 39–45.

Hrouda, F., 2004. Problems in interpreting AMS parameters in diamagnetic rocks. In: Martín-Hernández, F., Lüneberg, C.M., Aubourg, C., Jackson, M. (Eds.), Magnetic Fabric: Methods and Applications. Geological Society, London, Special Publications, vol. 238, pp. 49–59.

Ihmlé, P.F., Hirt, A.M., Lowrie, W., Dietrich, D., 1989. Inverse magnetic fabric in deformed limestones of the Morcles Nappe, Switzerland. Geophysical Research Letters 16, 1383–1386.

Jelinek, V., 1976. The Statistical Theory of Measuring Anisotropy of Magnetic Susceptibility of Rocks and Its Application. Geophysika, Brno.

Jelinek, V., 1981. Characterization of the magnetic fabric of rocks. Tectonophysics 79, 63–67.

Jelinek, V., 1985. The physical principles of measuring magnetic anisotropy with the torque magnetometer. Travaux Géophysique 33, 177–198.

Kligfield, R., Lowrie, W., Dalziel, I.W.D., 1977. Magnetic susceptibility anisotropy as a strain indicator in the Sudbury basin, Ontario. Tectonophysics 40, 287–308.

Kligfield, R., Owens, W.H., Lowrie, W., 1981. Magnetic susceptibility anisotropy, strain, and progressive deformation in Permian sediments from the Maritime Alps (France). Earth and Planetary Science Letters 55, 181–189.

Kligfield, R., Lowrie, W., Hirt, A., Siddans, A.W.B., 1983. Effect of progressive deformation on remanent magnetization of Permian redbeds from the Alpes Maritimes (France). Tectonophysics 97, 59–85.

Kocks, U.F., Tome, C.N., Wenk, H.-R., 1998. Texture and Anisotropy: Preferred Orientations in Polycrystals and Their Effect on Materials Properties. Cambridge University Press, p. 676.

Leiss, B., 2005. New techniques, measuring strategies and applications of conventional X-ray texture analysis. 15th conference on Deformation Mechanisms, Rheology and Tectonics, Zurich, Switzerland, p. 130.

Leiss, B., Ullemeyer, K., 2006. Neue Perpektiven der Texturanalytik von Gesteinen mit konventioneller Röntgenbeugung. In: Phillipp, S., Leiss, B., Vollbrecht, A., Tanner, D., Gudmundsson, A. (Eds.), 11. Symposium Tektonik, Struktur- und Kristallingeologie. Universitätsverlag Göttingen, Göttingen, Germany, pp. 128–130.

Lüneberg, C.M., Lampert, S.A., Lebit, H.D., Hirt, A.M., Casey, M., Lowrie, W., 1999. Magnetic anisotropy, rock fabrics and finite strain in deformed sediments of SW Sardinia (Italy). Tectonophysics 307, 51–74.

Mainprice, D., 1990. A FORTRAN program to calculate seismic anisotropy from the lattice preferred orientation of minerals. Computers and Geosciences 16, 385–393.

Mancktelow, N.S., 1985. The Simplon Line: a major displacement zone in the western Lepontine Alps. Eclogae Geologicae Helveticae 78, 73–96.

Mancktelow, N.S., 1990. The Simplon fault zone. Beiträge zur Geologischen Karte der Schweiz[NF] 163, 74.

Mancktelow, N.S., 1992. Neogene lateral extension during convergence in the central Alps: evidence from interrelated faulting and backfolding around the Simplonpass (Switzerland). Tectonophysics 215, 295–317.

Martín-Hernández, F., Hirt, A.M., 2001. Separation of ferrimagnetic and paramagnetic anisotropies using a high-field torsion magnetometer. Tectonophysics 337, 209–221.

Martín-Hernández, F., Kunze, K., Julivert, M., Hirt, A.M., 2005. Mathematical simulations of anisotropy of magnetic susceptibility of composite fabrics. Journal of Geophysical Research 110. doi:10.1029/2004JB003505.

Owens, W., Rutter, E., 1978. The development of magnetic susceptibility anisotropy through crystallographic preferred orientation in a calcite rock. Physics of the Earth and Planetary Interiors 16, 215–222.

Parés, J.M., van der Pluijm, B.A., 2002. Phyllosilicate fabric characterization by low-temperature anisotropy of magnetic susceptibility (LT-AMS). Geophysical Research Letters 29. doi:10.1029/2002GL015459.

Park, J.K., Tanczyk, E.I., Desbarets, A., 1988. Magnetic fabric and its significance in the 1400 Ma Mealy Diabase Dykes of Labrador, Canada. Journal of Geophysical Research 93, 13689–13704.

Ramsay, J.G., 1981. Tectonics and the Helvetic nappes. In: McClay, K.R., Price, N.J. (Eds.), Thrust and Nappe Tectonics. Geological Society of London Special Publications, vol. 9, pp. 293–309.

Ramsay, J.G., Casey, M., Kligfield, R., 1983. Role of shear in development of the Helvetic fold-thrust belt of Switzerland. Geology 11, 439–442.

Richter, C., van der Pluijm, B.A., 1994. Separation of paramagnetic and ferrimagnetic susceptibilities using low temperature magnetic susceptibilities and comparison with high field methods. Physics of the Earth and Planetary Interiors 82, 113–123.

Rochette, P., 1988. Inverse magnetic fabric in carbonate bearing rocks. Earth and Planetary Science Letters 90, 229–237.

Schmidt, V., Günther, D., Hirt, A.M., 2006. Magnetic anisotropy of calcite at room temperature. Tectonophysics 418, 63–73.

Schmidt, V., Hirt, A.M., Rosselli, P., Martín-Hernández, F., 2007a. Separation of paramagnetic and diamagnetic anisotropy by high-field, low-temperature torque measurements. Geophysical Journal International 168, 40–47.

Schmidt, V., Hirt, A.M., Hametner, K., Günther, D., 2007b. Magnetic anisotropy of carbonate minerals at room temperature and 77 K. American Mineralogist 92, 1673–1684.

Schmidt, V., Hirt, A.M., Leiss, B., Burlini, L., Walter, J.M., 2009. Quantitative correlation of texture and magnetic anisotropy of compacted calcite-muscovite aggregates. Journal of Structural Geology 31, 1062–1073.

Seward, D., Mancktelow, N.S., 1994. Neogene kinematics of the central and western Alps: evidence from fission-track dating. Geology 22, 803–806.

Siddans, A.W.B., Henry, B., Kligfield, R., Lowrie, W., Hirt, A.M., Percevault, M.N., 1984. Finite strain patterns and their significance in Permian rocks of the Alpes Maritimes (France). Journal of Structural Geology 6, 339–368.

Soom, M.A., 1990. Abkühlungs- und Hebungsgeschichte der Externmassive und der penninischen Decken beidseits der Simplon-Rhone-Linie seit dem Oligozän: Spaltspurdatierungen an Apatit/Zircon und K-Ar-Daterieungen an Biotit/Muskowit (Westliche Zentralalpen). PhD Thesis, University of Bern, Switzerland, p. 199.

Steck, A., 1984. Structures de déformations tertiaires dans les Alpes centrales (transversale Aar-Simplon-Ossola). Eclogae Geologicae Helveticae 77, 55–100.

Steck, A., Hunziker, J., 1994. The Tertiary structural and thermal evolution of the Central Alps - compressional and extensional structures in an orogenic belt. Tectonophysics 238, 229–254.

Trümpy, R., 1980. An outline of the geology of Switzerland. In: Geology of Switzerland, a Guidebook. International Geological Congress Guidebook 10. Wepf and Co., Basel, p. 104.

Wenk, H.-R., Matthies, S., Donovan, J., Chateigner, D., 1998. BEARTEX: a Windows-based program system for quantitative texture analysis. Journal of Applied Crystallography 31, 262–269.